Chemistry–A European Journal
Research Article
doi.org/10.1002/chem.202303994
Chemistry Europe
European Chemical Societies Publishing
www.chemeurj.org

Highly Ordered Co-Assembly of Bisurea Functionalized Molecular Switches at the Solid-Liquid Interface

Cosima Stähler[+],[a] Robby Reynaerts[+],[b] Tamara Rinkovec,[b] Lander Verstraete,[b, c] G. Henrieke Heideman,[a] Andrea Minoia,[d] Jeremy N. Harvey,[b] Kunal S. Mali,*[b] Steven De Feyter,*[b] and Ben L. Feringa*[a]

Immobilization of stimulus-responsive systems on solid surfaces is beneficial for controlled signal transmission and adaptive behavior while allowing the characterization of the functional interface with high sensitivity and high spatial resolution. Positioning of the stimuli-responsive units with nanometer-scale precision across the adaptive surface remains one of the bottlenecks in the extraction of cooperative function. Nanoscale organization, cooperativity, and amplification remain key challenges in bridging the molecular and the macroscopic worlds. Here we report on the design, synthesis, and scanning tunneling microscopy (STM) characterization of overcrowded alkene photoswitches merged in self-assembled networks physisorbed at the solid-liquid interface. A detailed anchoring strategy that ensures appropriate orientation of the switches with respect to the solid surface through the use of bis-urea groups is presented. We implement a co-assembly strategy that enables the merging of the photoswitches within physisorbed monolayers of structurally similar 'spacer' molecules. The self-assembly of the individual components and the co-assemblies was examined in detail using (sub)molecular resolution STM which confirms the robust immobilization and controlled orientation of the photoswitches within the spacer monolayers. The experimental STM data is supported by detailed molecular mechanics (MM) simulations. Different designs of the switches and the spacers were investigated which allowed us to formulate guidelines that enable the precise organization of the photoswitches in crystalline physisorbed self-assembled molecular networks.

Introduction

Molecular self-assembly, ubiquitous in nature offers a convenient way of making complex supramolecular architectures held together *via* non-covalent bonds.[1] For decades, researchers have aspired to build artificial materials *via* molecular self-assembly that rival the complexity and perfection of natural systems.[2–3] It is widely acknowledged that self-assembled materials that mimic the intricacy of natural systems will enable next generation technologies in diverse fields ranging from renewable energy and smart materials to advanced medicine.[4–11]

One of the most burgeoning research areas in the context of mimicking the dynamic functions of natural systems is that of artificial molecular switches, motors and machines.[12–21] Inspired by the efficiency of complex biological systems and supported by the advances in synthetic chemistry, chemists have fabricated artificial systems comprising mechanically interlocked molecules,[13,22–23] molecular motors[24] and molecular switches[17,25–27] capable of executing functions reminiscent of those of their biomolecular counterparts. These systems are driven by external stimuli such as chemical or electrochemical reactions,[28] changes in the pH,[29] electric field[30] and light.[31–32] Dynamic systems that respond to light irradiation are particularly appealing because light can be delivered with high spatiotemporal precision without producing chemical waste in the photochemical process in a non-invasive fashion.[19,33]

Many investigations on molecular motors have been carried out in solution. However, when operated as small molecules in solution, their movement is overwhelmed by Brownian motion.[34] Anchoring motors and switches on solid surfaces as immobilization strategy limits the degrees of freedom available to the molecules and bestows a certain degree of order.[35] The surface immobilization strategy not only provides a convenient way of interfacing the motors and switches with the macroscopic world, but also allows scaling up of the motion generated at the nanoscale so as to perform work.[36–37]

Given that immobilization of molecular motors on solid surfaces is a key step towards fabrication of devices that can exploit their collective motion, different anchoring strategies

[a] C. Stähler,[+] G. H. Heideman, B. L. Feringa
Stratingh Institute for Chemistry, University of Groningen, Nijenborgh 4, 9747 AG Groningen, The Netherlands
E-mail: b.l.feringa@rug.nl
[b] R. Reynaerts,[+] T. Rinkovec, L. Verstraete, J. N. Harvey, K. S. Mali, S. De Feyter
Division of Molecular Imaging and Photonics, Department of Chemistry, KU Leuven, Celestijnenlaan 200F, B-3001 Leuven, Belgium
E-mail: kunal.mali@kuleuven.be
steven.defeyter@kuleuven.be
[c] L. Verstraete
imec, Kapeldreef 75, 3001 Leuven, Belgium
[d] A. Minoia
Laboratory for Chemistry of Novel Materials, Materials Research Institute, University of Mons, Place du Parc 20, 7000 Mons, Belgium
[+] equal contributions

Supporting information for this article is available on the WWW under https://doi.org/10.1002/chem.202303994

have been developed. Overcrowded alkene-based motors have been anchored onto quartz[38–39] and gold[40–42] substrates and both covalent and non-covalent immobilization approaches have been employed. Immobilization was achieved by introducing two or more "legs" with specific functional groups to the motors, designed to bind the surface *via* covalent bonds[38,40,43] or non-covalent interactions.[39,44]

Despite the potential of the surface anchoring approach, pre-programmed self-assembly of overcrowded alkenes, where precise positional and orientation control on the rotors is achieved, remains to be demonstrated. In this context, a physisorption approach, where the building blocks interact with the solid substrate *via* relatively weak non-covalent interactions and undergo further two-dimensional (2D) self-assembly *via* additional non-covalent interactions is promising. The weaker interactions involved in the process often allow dynamic healing of defects thereby enabling the formation of crystalline physisorbed self-assembled molecular networks (SAMNs).[45]

Furthermore, provided that the information of the ensuing supramolecular interactions is encoded in the molecular structure *via* a judicious choice of structural features such as functional groups, substitution patterns, and stereogenic centers, it is possible to build hierarchically complex architectures with nanoscale control over the structure and composition.[45–46] Such control, if exercised over the assembly of rotors and switches can help in engineering coherent molecular motion at the nano- and the macroscopic scale.

Building on previously developed anchoring strategies, in particular our studies on precise self-organization of functional molecular systems on solid substrates,[47–48] and using the principles of 2D-crystal engineering, in this contribution, we report a co-assembly approach for merging overcrowded alkene photoswitches in physisorbed monolayers formed at the solution-graphite interface (Scheme 1). Among other things, it features the incorporation of bisurea units flanking the central functional molecular switch and takes advantage of the propensity to precisely organize the individual molecules in well-aligned 2D tapes due to the array of the bisurea hydrogen-bonds. A detailed design strategy, which includes the design of the molecular switch as well as the overall supramolecular design required for the co-assembly of the switch with a so-called 'spacer' molecule used for creating the required free volume for the unobstructed motion of the switch, is presented. Multiple designs for the photoswitch and the spacer were considered (Scheme 2) and their synthesis is described (Scheme 3). The self-assembly of individual components as well as different spacer-switch combinations was thoroughly characterized using STM at the solution-solid interface. Detailed molecular mechanics (MM) simulations were employed to confirm the desired orthogonal orientation of the switch with respect to the graphite surface. We conclude with selected designs that allow flawless merging of the photoswitches in crystalline physisorbed SAMNs. These structures enable the precise arrangement of switches in robust, yet dynamic SAMNs. This advancement opens up possibilities for light-induced switching of overcrowded alkenes confined to solid surfaces in the future.

Results and Discussion

Design

Several structural parameters were considered for the molecular as well as the supramolecular design. One of the most important criteria is the decoupling of the rotor from the substrate surface and other rotors in the vicinity, to eventually harness the rotary motion in an unhindered manner.[41] Secondly, since ordered arrays of molecular switches are desired, structural features that enable robust binding of the

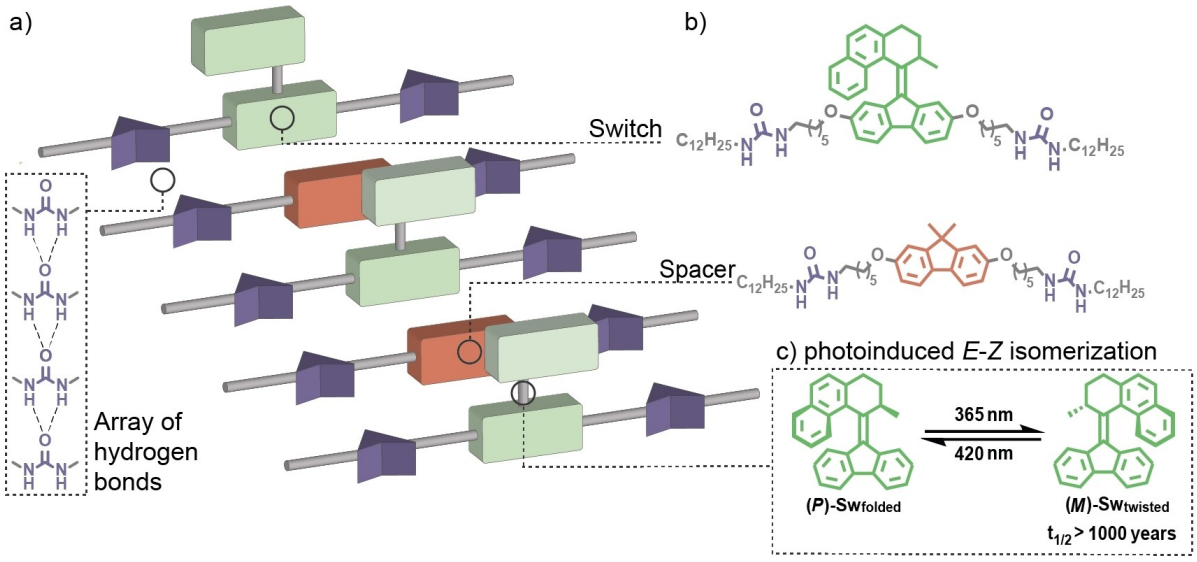

Scheme 1. (a) Proposed co-assembly strategy. (b) Molecular structures of a photoswitch and a spacer molecule. For the complete list of switches and spacers, see scheme 2. (c) Photochemical *E-Z* isomerization of the photoswitch.

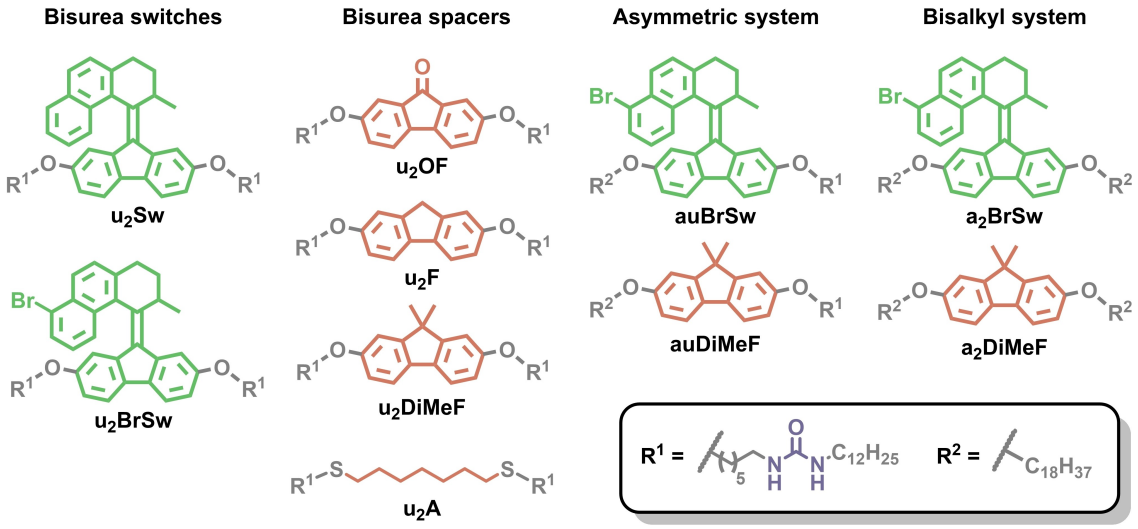

Scheme 2. A pool of functional molecules designed, synthesized and studied in this work. Abbreviations: u = ureidoalkyl chain, a = alkyl chain (terminal), Sw = switch, BrSw = bromoswitch, OF = fluorenone, F = fluorene, DiMeF = dimethylfluorene, A = alkyl chain in the center of the molecule.

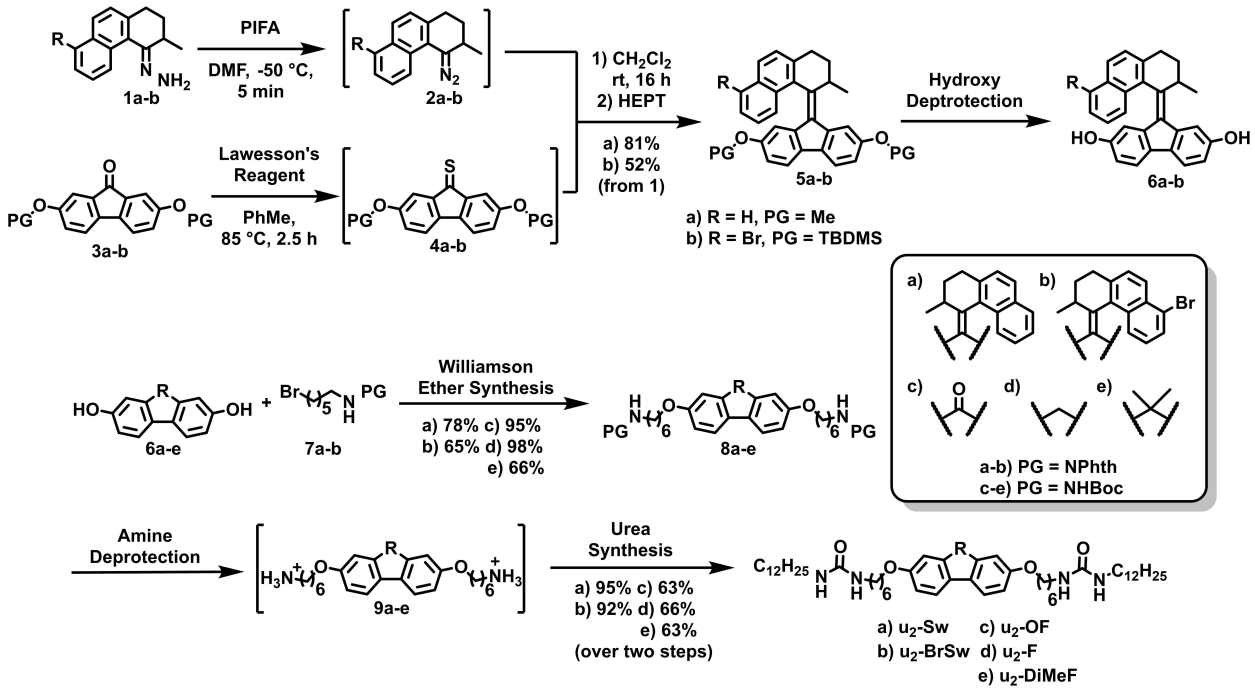

Scheme 3. Two protected hydroxyl substituted switches were formed *via* a Barton-Kellogg olefination. Deprotection of the methoxy switch was achieved in neat CH_3MgI and deprotection of the TBS groups was performed with LiOH in DMF. The side chain functionalization starts with a Williamson ether synthesis (K_2CO_3, MeCN, reflux, overnight) and the introduction of a protected amine. Next, the amine was deprotected (TFA, CH_2Cl_2, room temp. for Boc and Hydrazine monohydrate in ethanol reflux for phthalimide) and immediately used in a urea synthesis (dodecylisocyanate in CH_2Cl_2 and trimethylamine).

switch to the surface and their supramolecular ordering through strong and directional intermolecular interactions maintaining proper orientation have to be implemented. The key features of our design are highlighted in Scheme 1.

Graphite was chosen as the substrate since it allows relatively straightforward adsorption and 2D self-assembly of typical organic molecules on its basal plane.[45] Highly oriented pyrolytic graphite (HOPG) presents atomically flat large terraces that facilitate the characterization of SAMNs using STM under ambient conditions. Long alkyl chains/alkanes are known to interact favorably with the basal plane of graphite. Linear alkanes form close-packed 2D lamellae on graphite, which are stabilized *via* molecule-surface and molecule-molecule van der Waals (vdW) interactions. In fact, vdW interactions between close-packed (interdigitated) alkyl chains is one of the routinely employed design elements in on-surface supramolecular chemistry.[49] Although vdW interactions intrinsically lack the strength and directionality of H-bonds, when used in combina-

tion with an appropriate surface and molecular design strategy, they are extremely effective in directing surface self-assembly.[50–51] Thus alkylation of the photoswitch was considered as the first design element.

To impart additional robustness and directionality to the SAMNs, incorporation of bis-urea units to the alkyl chains was considered as the second design element. The urea group is a strong H-bonding unit and the cooperativity of H-bonding between two urea groups has been intensively used in supramolecular chemistry.[52–53] Bis-urea derivatives are known to form ladder-like supramolecular assemblies both in solution and on surfaces. The self-assembly leads to the formation of lamellar structures at the solution-graphite interface.[54–55] Due to strong intermolecular H-bonding, the SAMNs formed by bis-urea derivatives are remarkably stable, even allowing stabilization and STM imaging of isolated lamellae at the solution-graphite interface.[56] Furthermore, our previous work on bis-urea derivatives carrying thiophene units indicated that the thiophene cores are well organized and do not lie flat but are tilted with respect to the surface.[54] This is promising for the current design, since an approximately orthogonal orientation of the molecular switch relative to the surface is desired to retain the switching ability upon surface immobilization.

Scheme 2 shows the molecular structure of the bistable switch designed and synthesized for our studies. The central part consists of the overcrowded alkene motif. Due to steric hindrance between the stator and the rotor halves, the switch adapts a non-planar conformation. The methyl group on the rotor, at the stereocenter of the switch, acquires a pseudo-axial orientation in its initial state. At this orientation, the *R* enantiomer expresses itself with a *P* helicity while the *S* enantiomer with an *M* helicity. The switch is synthetically obtained as a racemic mixture, which is not separated for this study. The stator is symmetrically substituted with ureidoalkyl chains (**u_2Sw**, Scheme 2). A number of structural variations of this basic design were also synthesized. A bromine substituted derivative (**u_2BrSw**, Scheme 2) was prepared anticipating that the halogen substituent will allow better visualization of the orientation and directionality of the switch relying on the enhanced contrast of halogens in STM images.[57–58] To validate the design containing the bis-urea groups, two structurally similar switches, namely a bis-alkyl switch (**a_2BrSw**), and a switch featuring an alkyl chain on one side and an ureidoalkyl on the other (**auBrSw**) were synthesized (Scheme 2).

The last but arguably the most important design element concerns the creation of free volume around the rotor. If the bis-urea appended molecular switches self-assemble in a columnar fashion, then the rotors will be placed too close to each other along the column axis thereby hampering their motion. To alleviate this hurdle, a set of structurally similar molecules resembling the stator was designed. The idea is that this molecule, hereon referred to as the 'spacer' co-assembles at the surface, and creates the required free volume around the rotor by merging in between the switches within the SAMN. To this end, a set of fluorene-based spacers with the same variety of side chains was synthesized. The fluorene core resembles the stator of the switch and hence we envisioned stabilization of the spacer-switch co-assembly *via* π-stacking interactions in addition to the H-bonding interactions between the bis-urea moieties. The (ureido)alkyl chains thus separate the rotors along a direction perpendicular to the column axis whereas the fluorene cores separate them along the column axis. To manipulate the steric bulk of the spacer, and in turn the free volume around the rotor, a few structural variations of the fluorene cores were considered. For example, the spacer with dimethyl fluorene core (**u_2DiMeF**) has a slightly larger steric bulk compared to the spacer with fluorene (**u_2F**) or fluorenone (**u_2OF**) core (Scheme 2). Furthermore, to evaluate the influence/importance of the fluorene core, a corresponding bis-urea alkyl spacer (**u_2A**) lacking this unit was also prepared. Similar to that for the switch, bis-alkyl (**a_2DiMeF**) and mono-urea (**auDiMeF**) variations were also synthesized.

Synthesis

Asymmetric second-generation overcrowded alkene-based molecular motors and switches are typically prepared by a Barton-Kellogg olefination between a thioketone and a diazo compound (Scheme 3).[59] The rotor was first synthesized as the corresponding hydrazone following literature procedures[60] and used to form the diazo compound upon (*bis*(trifluoroacetoxy)iodo)benzene (PIFA) oxidation. For the lower half of the unsubstituted switch **5a**, 2,7-dimethoxyfluorenone (**3a**) was treated with Lawesson's reagent to prepare thioketone **4a**, which was coupled with diazo compound **2a**. Desulphurization of the resulting episulfide with hexaethylphosphorous triamide (HEPT) afforded the switch **5a** in a good overall yield of 81%. For the brominated switch **5b**, a *tert*-butyldimethylsilyl (TBS) protected fluorenone **3b** was used and subjected to the same reaction conditions with diazo compound **2b**, affording the desired product in an overall yield of 52%. In the next steps the deprotection of the methoxy groups for **5a** was achieved using neat methyl magnesium iodide while LiOH was used for the TBS groups of **5b**, respectively. Both switches are obtained as enantiomeric mixtures of *M* and *P* helicity and are used as such for the surface studies.

For the spacers, four different functionalities were synthesized and investigated: fluorenone **u_2OF**, fluorene **u_2F**, dimethylfluorene **u_2DiMeF** and a thioether alkyl spacer **u_2A**. Starting from 2,7-dihydroxyfluorenone, 2,7-dihydroxyfluorene and 2,7-dihydroxydimethylfluorene were obtained following literature procedures[61–64](see supporting information, section 2.1.) and submitted to the side chain functionalization. The side chain attachment was achieved for all five molecules in a similar fashion. Starting with a Williamson ether synthesis, a protected amine is introduced. The amine was protected with a *tert*-butyloxycarbonyl (Boc) protecting group in the case of the fluorine-based spacers, which was removed using trifluoro acetic acid (TFA). As overcrowded alkenes can be acid-sensitive, a phthalimide protecting group was introduced for **8a** and **8b** and removed upon treatment with hydrazine. The urea functionality was formed upon the reaction of the free amine with dodecylisocyanate (see supporting information, section

2.2.). The aliphatic spacer **u_2A** was synthesized starting from dithiol[65] and attachment of a phthalimide functionalized side chain *via* a thioether synthesis. Amine deprotection and reaction with dodecylisocyanate afforded **u_2A** (see supporting information, section 2.5.). Aliphatic thioethers are generally more accessible synthetically than their ether counterparts. For the assembly we expect no difference between a thioether or ether, as the hydrogen bonding will form the primary interaction between the molecules.

The compounds featuring urea functionalized spacers all precipitated from the final reaction mixture in dichloromethane and could simply be filtered and purified by washing. Analysis of the spacer molecules by ^{1}H NMR had to be performed at elevated temperatures, as the spacers would form gels upon dissolution in high-boiling solvents under heating (see supporting information, section 3), making the analysis of the solution at room temperature difficult. Interestingly, the fully functionalized switches **u_2-Sw** and **u_2-BrSw** could be purified by column chromatography, as they are perfectly soluble in various solvents and do not precipitate upon formation.

Additionally, bis-alkylated switch **a_2BrSw** and bis-alkylated spacer **a_2DiMeF** (see supporting information, section 2.4. and 2.11.), were synthesized using a Williamson ether synthesis with bromododecane. Asymmetric surface molecules with one alkyl and one bisurea chain (**auBrSw** and **auDiMeF**) were synthesized by installing the urea chain as before, subsequently to the introduction of the alkyl chain (see supporting information, section 2.3. and 2.12.). **auBrSw** was obtained as a mixture of *E* and *Z* forms and used as such for the surface studies without separation of the isomers.

On-surface self-assembly

Self-assembly of the spacers

Since the spacers are expected to 'hold' the molecular switches in place in an appropriate orientation with respect to the surface, the on-surface self-assembly of the spacers was first studied in detail. Comparison of the assembly behavior of the different designs (Scheme 2) allowed us to make an informed choice of a spacer molecule by understanding the influence of the different features implemented in the spacer design described earlier. We present two representative cases below which illustrate the influence of the urea functionality on the self-assembly behavior and its importance in the eventual supramolecular design.

Figure 1 shows comparison of the self-assembly behavior of the bis-urea (**u_2DiMeF**) and the bis-alkyl (**a_2DiMeF**) derivatives with the same cores namely, dimethylfluorene, at the solution-graphite interface. A large-scale STM image provided in Figure 1a shows the SAMN formed by **u_2DiMeF** at the octanoic acid-HOPG interface. As previously reported for bis-urea derivatives,[54] the network consists of lamellar organization of molecules in which the relatively bright appearing lamellae are separated by dark troughs. Lamellae in the adjacent domains are oriented at approximately 60° or 120° with respect to each other, reflecting the influence of the symmetry of the underlying graphite lattice on the self-assembly. The high-resolution STM image provided in Figure 1b shows that each lamella consists of a central bright ridge (blue arrow) flanked on either side by striped features that run approximately perpendicular to the long axis of the column. We attribute the central bright features to the dimethylfluorene units and the striped features with darker STM contrast to the ureidoalkyl chains. Furthermore, two ridges with an intermediate contrast that run along the lamella axis (red arrows) can also be discerned, which can be ascribed to the H-bonded urea groups.[54] The width of the lamella is 6.4 ± 0.1 nm which indicates that the ureidoalkyl chains are arranged end-to-end and not interdigitated. The distance between the adjacent ureidoalkyl chains along the lamella axis is 0.5 ± 0.1 nm which indicates that the assembly is dominated by the H-bonding interactions between the ureidoalkyl chains despite the presence of the bulky dimethylfluorene cores. This implies that the dimethylfluorene cores may not have enough space to lie flat (face-on)[66] but may adsorb at an angle (edge-on) with respect to the graphite surface. A tentative molecular model based on calibrated STM data is provided in Figure 1c. It assumes an approximately orthogonal orientation of the dimethylfluorene core with respect to the surface and can reproduce the symmetry and periodicity evident from the STM data.

Figure 1d shows a representative large-scale STM image of **a_2DiMeF** SAMN formed at the OA/HOPG interface. One immediately noticeable difference between the self-assembly of **u_2DiMeF** and **a_2DiMeF** is the size of the domains. **a_2DiMeF** forms much larger domains compared to **u_2DiMeF** which could be related to the better solubility of the former. The large-scale STM image shows wavy rows of bright features separated by darker troughs. The high-resolution STM image provided in Figure 1e shows a ladder-like network in which the bright features are connected to each other *via* stripes of darker contrast. The width of the lamella is 3.2 ± 0.1 nm which is half of that observed for **u_2DiMeF**. While a slight reduction in the width of the lamellae was anticipated compared to that of the **u_2DiMeF**, the significant decrease in the observed lamella width indicates a fundamentally different packing for **a_2DiMeF**. Furthermore, rows of bright features which we attribute to the dimethylfluorene cores appear to be shifted after propagating a certain distance along the lamella axis. These shifts occur after every 5,7-dimethylfluorene cores. SAMNs with such fractured arrangement of molecules have been reported by us in the past. In the case of those systems, the origin of such shifts was found to lay in the maximization of close packing of molecules on the surface.[67–68] A molecular model built based on the unit cell parameters obtained from the calibrated STM data is presented in Figure 1f. The much smaller width of the lamellae indicate that the alkyl chains are interdigitated. This contrasts with **u_2DiMeF** where they are arranged end-to-end. The interdigitation leaves enough space for the dimethylfluorene core to adsorb face-on and consequently the central part of the lamellae is relatively better resolved compared to that in **u_2DiMeF**.

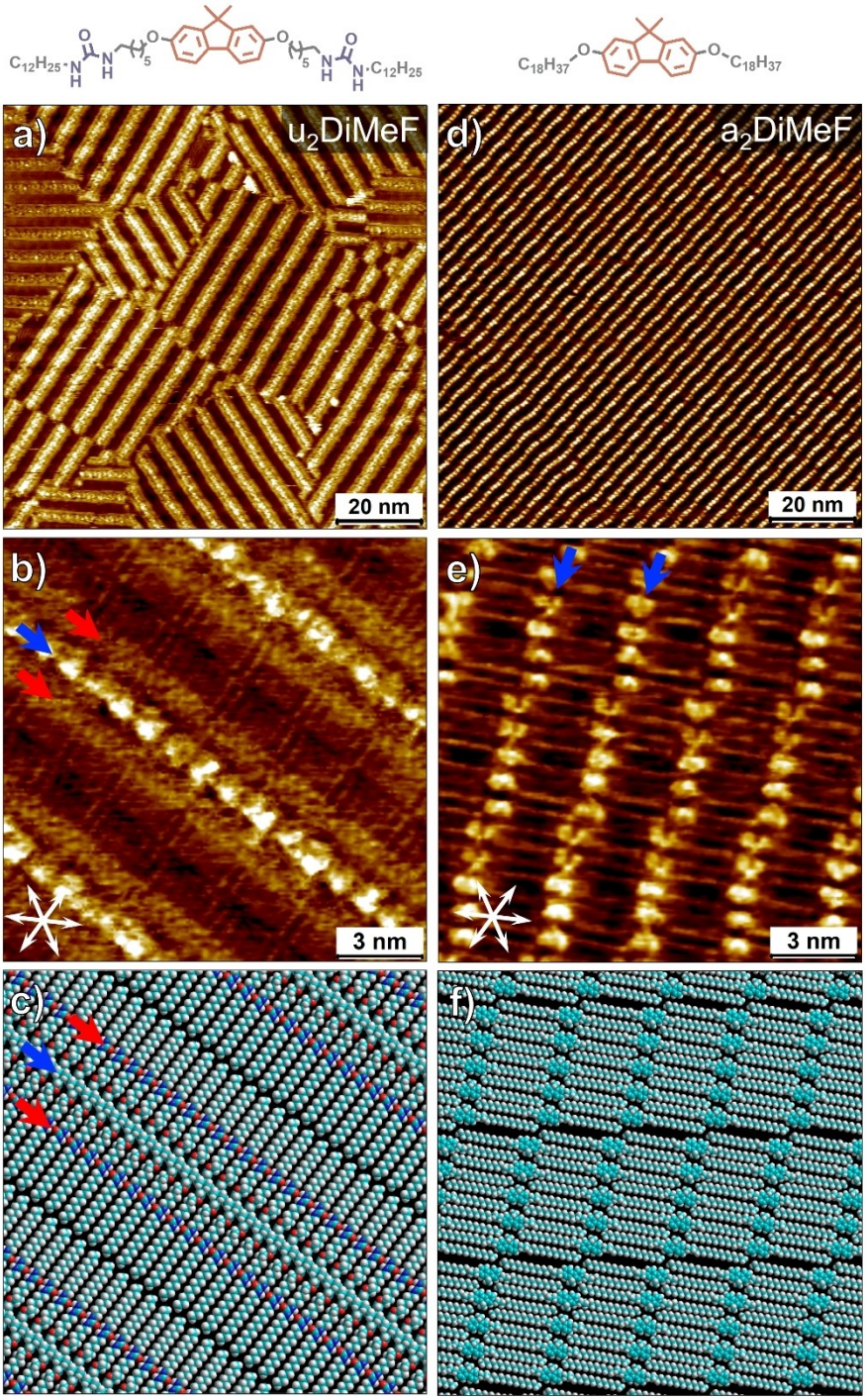

Figure 1. Comparison between the self-assembly of the bis-urea (u_2DiMeF, a-c, 0.5 mM) and the bis-alkyl (a_2DiMeF, d–f, 0.5 mM) dimethyl fluorene spacers at the OA/HOPG interface. (a, d) Large scale STM images. (b, e) High-resolution STM images. (c, f) Tentative molecular models based on the calibrated STM data. Blue arrows indicate the position of the dimethylfluorene cores whereas the red arrows in (b) and (c) indicate the positions of the H-bonded urea units. The symmetry axes of the graphite lattice are displayed in the lower left corners of (b) and (e). Imaging parameters: (a) $V_{bias} = -0.93$ V, $I_{set} = 0.09$ nA. (b) $V_{bias} = -0.80$ V, $I_{set} = 0.05$ nA. (c, d) $V_{bias} = -1.4$ nA, $I_{set} = 0.10$ nA.

The appearance of dimethylfluorene cores differs from molecule to molecule and the origin of this contrast difference is unclear. It could be related to the different orientations of the cores along the column axis. The **a_2DiMeF** molecules can adsorb on either face and thus the direction in which the methyl groups are facing along the column axis can be different. Given the larger space allowed for adsorption of the cores due to the interdigitation of the alkyl chains, both such orientations are possible. Such variation is less likely in the case of the **u_2DiMeF**, due to the highly directional H-bonding known for the bis-urea systems. The comparison between the two spacers already underscores the importance of the bis-urea

functionality in the desired supramolecular design. It enables robust arrangement of spacers on the surface *via* directional H-bonding which in turn reduces defects and also plausibly allows the desired edge-on arrangement of the spacer molecules.

To substantiate the orientation of the dimethylfluorene units with respect to the surface, detailed MM calculations were performed (see supporting information, section 4). Given the flexible nature of the side chains, the conformations of isolated single molecules in vacuum were first studied using MM based geometry optimization. This provided multiple geometries where the conformers differ in terms of the relative orientation of the dimethylfluorene core with respect to the alkyl chains. The most stable geometry for an isolated single molecule in vacuum is found to be the one in which the torsion angle of the dimethylfluorene unit relative to the alkyl chains is 0° and where the two urea groups point in the opposite direction (Figure S2 in the supporting information). Additionally, it was noted that the relative stability of the conformers depends significantly on the torsion parameters used for the previously described torsion angle. Therefore, the MM calculations described here were performed using a modified OPLS-AA force field in which the torsional parameters for this bond were reparametrized based on B3LYP-D3 calculations for 2,7-dimethoxy-9,9-dimethyl-9H-fluorene (Table S1 in the supporting information).

To study the assembly behaviour of the spacer molecules on the graphite surface, molecular models were built based on the unit cell parameters obtained from the calibrated STM data. This was repeated for all the different conformations. For edge-on conformations, two different orientations with respect to the graphene surface were recognised due to the symmetry of the dimethylfluorene core: one where the fluorenyl methyl groups point towards the surface and another where they point away from it (see Tables S2-S3 in the supporting information). Solvent was not considered in the MM calculations. While results below discuss the energies obtained from MM geometry optimization, molecular dynamics simulations of the monolayers were performed in order to generate starting points for the minimization and in order to ensure that realistic minima were located.

Figure 2a, b shows the MM optimized structure of the most stable SAMN on the graphene surface. This structure was obtained when starting with a conformer where the torsion angle between the dimethylfluorene core and the ureidoalkyl chain was 84° with methyl groups pointing away from the graphene surface (see Table S4 in the supporting information). However, irrespective of whether the input structures were based on face-on or edge-on conformations, geometry optimization always led to a change in the orientation of the dimethylfluorene units with respect to the surface in all systems. In general, these units adopted an edge-on configuration with varying degrees of tilt with respect to the surface. Since the assembly is held together by H-bonding, the position of the urea groups in the chain dictates the interchain distance. As described earlier, the geometric constraint enforced by H-bonding means that the dimethylfluorene cores need to adjust by tilting with respect to the graphene surface. MM calculations indicate that it is relatively easier for the edge-on conformations to adapt to this constraint which is reflected in their stabilization energies (see Table S2 in the supporting information). Furthermore, the orientation of the urea groups within a molecule (*syn* or *anti*, see Figure S2 in the supporting information) chains was also found to influence the overall stabilization energy. The *syn* conformation for our systems is favored, as expected for systems with an uneven number of atoms in the chain between the urea groups. The MM calculations thus clearly reveal that the preferred structure for the **u_2DiMeF** SAMN is the one where the dimethylfluorene units adsorb in an edge-on fashion approximately orthogonal to the surface as desired from the design principles outlined earlier.

The SAMNs formed by the bis-alkyl spacer were also studied using MM calculations for the sake of comparison. In these calculations, however, the length of the alkyl chains was set to 21 carbon atoms (**a_2DiMeF-C21**) to match the length of

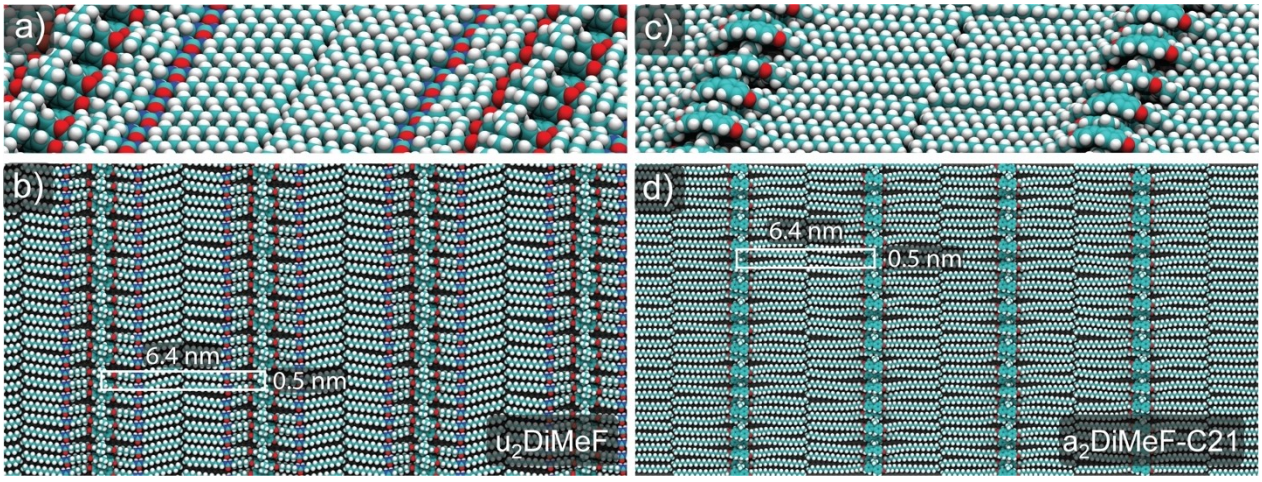

Figure 2. MM optimized molecular models for the SAMNs formed by the bis-urea and the bis-alkyl spacers. (a, b) u_2DiMeF (c, d) a_2DiMeF-C21. It is clear from the models for u_2DiMeF that the dimethylfluorene units are adsorbed edge-on whereas for a_2DiMeF-C21 their orientation is predominantly face-on with large disorder in the SAMN.

u_2DiMeF. The outcome of the MM calculations revealed that the most stable structure for the bis-alkyl spacer is the one in which the dimethylfluorene units adsorb almost face-on on the surface, though due to spatial constraints, the fluorenyl units slightly overlap each other (Figure 2c, d). The obtained network is stabilized by van der Waals interactions between the alkyl chains which are closely packed. Geometry optimization also led to the partial overlap between the dimethylfluorene units. The MM calculations reproduce the periodic gaps observed between the alkyl chains in the STM data (compare Figure 2d and Figure 1e, f). The face-on adsorption for the bis-alkyl spacer predicted by MM calculations further validates the choice of the bis-urea motifs in the final design.

The experimental self-assembly of the additional spacer designs was also studied in detail using STM. The STM data is presented in section 5 of the supporting information. Both **u_2F** and **u_2OF** form stable SAMNs at the solution/graphite interface which resemble closely to that of **u_2DiMeF** (Figure S4–S5 in the supporting information). However, they were not studied in detail later on as spacer/switch combinations because preliminary data suggested that merging of the photoswitches within the lamellae of spacers was poor, plausibly due to strong π-stacking interactions within the spacers themselves. The **u_2A** spacer also formed stable, long-range ordered SAMNs but it was also not studied in detail due to poor mixing with the photoswitch (Figure S6 in the supporting information). The self-assembly of the spacer carrying an alkyl chain on side and an ureidoalkyl chain on the other, yielded somewhat ill-defined networks (Figure S7 in the supporting information).

Self-assembly of the photoswitches

Figure 3 shows the STM images of SAMNs formed by the two bis-urea switches (**u_2Sw** and **u_2BrSw**) and the bis-alkyl (**a_2BrSw**) switch. As expected from the strong steric hindrance between the rotor parts of the closely packed molecules, the self-assembled networks were found to be relatively less ordered compared to those of the bis-urea spacers. Obtaining molecular resolution on SAMNs of photoswitches was extremely challenging. While a few images revealed arrangement of the rotors along the center of the lamellae for **u_2Sw** (Figure 3a, b), the monolayers of **u_2BrSw** were rather poorly resolved (Figure 3c, d). For the former, the distance between the rotors along the column axis varies between 0.5 nm and 1.5 nm. The width of the lamellae for both the systems was found to be 6.3 ± 0.2 nm, which matches closely with that of **u_2DiMeF**. In contrast to the SAMNs of the spacers, the switch assembly was found to be rather dynamic on the time scale of STM measurements with movement of entire domains observed in subsequent STM scans (Figure S8 in the supporting information).

Similar to the bis-alkyl spacers, the bis-alkyl brominated switch **a_2BrSw** also assembles in a lamellar structure with interdigitating alkyl chains (Figure 3e, f). The width of the

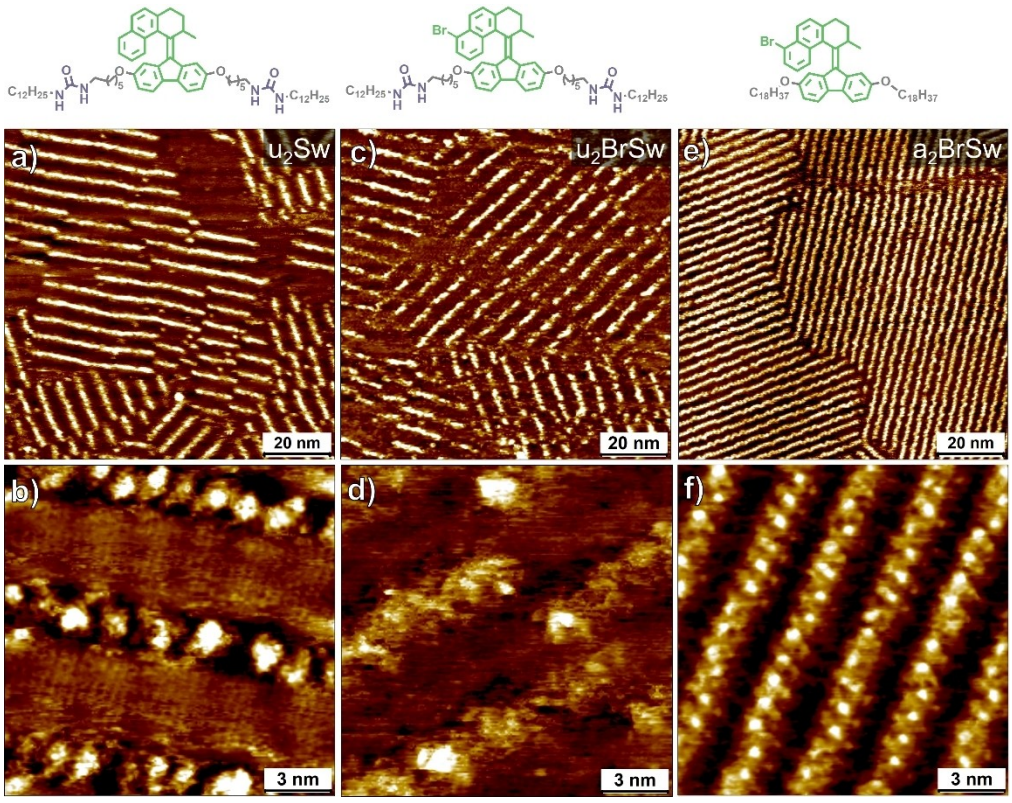

Figure 3. Self-assembly of the bis-urea and bis-alkyl photoswitches at the solution-solid interface. (a, b) u_2Sw (0.05 mM). (c, d) u_2BrSw (0.05 mM). (e, f) a_2BrSw (0.5 mM). Imaging parameters: (a) $V_{bias} = -0.80$ V, $I_{set} = 0.05$ nA. (b) $V_{bias} = -0.90$ V, $I_{set} = 0.01$ nA. (c, d) $V_{bias} = -1.40$ V, $I_{set} = 0.12$ nA. (e, f) $V_{bias} = -1.40$ V, $I_{set} = 0.02$ nA.

lamellae is 3.1 ± 0.1 nm. The lamellae consist of central bright rows which exhibit an irregular wavy pattern of bright circular features. These features can be attributed to the rotors which are leaning left or to the right of each lamella (Figure 3f). The average domain sizes were found to be much larger compared to those of the bis-urea switches. The photoswitch with the mixed chain system (**auBrSw**) formed only disordered assemblies which were extremely challenging for imaging, plausibly because of their dynamic nature on the surface (Figure S9 in the supporting information).

Co-assembly of the photoswitches and spacers: u_2DiMeF/u_2Sw and u_2DiMeF/u_2BrSw systems

The formation of crystalline long-range ordered multicomponent SAMNs upon mixing of two or more building blocks at the solution-solid interface is often a non-trivial process. Therefore, before describing the co-assembly experiments, we first discuss the possible outcomes when more than one building block is brought at the solution-solid interface: (1). *Phase separation:* In this case, both the molecules adsorb however, each molecule forms a separate domain of its own. (2). *Random mixing:* Here, both the molecules adsorb but one of the molecules is randomly distributed within the crystalline domains formed by the other molecule without significantly disturbing the unit cell of the latter. Such mixing occurs when the two building blocks have identical unit cell parameters, except for the unusual case of 2D solid solutions.[69] (3). *Co-crystallization:* In this case, the molecules form a crystalline matrix with a defined surface stoichiometry. Typically, co-crystallization occurs as a result of strong intermolecular interactions such as hydrogen bonding or space filling constraints as observed for host-guest systems.[70] (4) *Preferential adsorption:* A fourth possibility, often encountered when molecules self-assemble at the solution-solid interface, is that of preferential adsorption. Here, one component adsorbs on the surface whereas the other one is left in the solution phase. In general, multicomponent self-assembly at the solution-solid interface is strongly governed by both the symmetry and the quantitative similarity of the unit cells as well as the compatibility of the functional groups of the constituent building blocks.

Based on the discussion provided above and defined by the design principles discussed earlier, random mixing of the photoswitches within the spacer SAMN is anticipated. Initial co-assembly experiments were focused on the **u_2DiMeF** spacer and the **u_2Sw** mixtures (see section 5.1. in the supporting information for experimental details). Figure 4a, b shows the STM images of the SAMN obtained after the deposition of a solution containing an equimolar solution of **u_2DiMeF** and **u_2Sw**. The large-scale STM image shows lamellar features typical of the spacer self-assembly (see Figure 1a) however differs in the STM contrast along the center of the lamellae. The lamella axis typically shows significant variation in the contrast with interspersed bright features. This is indicative of the merging of the photoswitches (**u_2Sw**) within the SAMN of the spacer (**u_2DiMeF**). Figure 4b shows an STM image where single photoswitches can be discerned within the SAMN of spacers. A few switch molecules are highlighted with colored squares and the corresponding digital zooms are provided next to the STM image (Figure 4 i–iii). These images reveal that the photoswitch can be immobilized upon merging within the monolayer of the spacer. Furthermore, the zoomed-in data also shows sub-molecular features where a single photoswitch is typically imaged as a four-leaf clover (Figure 4b, green, i). The isolated photoswitches also exhibit other types of contrast in STM images (Figure 4b, red, blue, ii and iii). The origin of this contrast difference is unclear. The photoswitches are positioned approximately in the middle of the spacer lamella (*vide infra*: directionality). They do not cause any visible defect within the SAMN of the spacer indicating their seamless insertion within the lamella *via* H-bonding interaction with the spacers. The submolecular resolution obtained in the STM images also indicates that the immobilization of the switch is robust on the time scale of STM imaging (also see section 3.3.2 below).

The co-assembly behavior of the brominated switch (**u_2BrSw**) with **u_2DiMeF** (Figure 4c, d) matches closely to that of the non-brominated switch except for one major difference. The average number of switches observed per unit area on the graphite surface is higher for the **u_2DiMeF/u_2BrSw** system (see next section 3.3.1. below). This contrasts with the self-assembly behavior of the **u_2BrSw** switch above, which furnished rather dynamic monolayers unstable to STM scanning. The **u_2BrSw** molecules are well-merged within the **u_2DiMeF** lamellae and also exhibit four-lobed STM contrast as that of the non-brominated switches (Figure 4d, colored squares iv–ix).

Co-assembly of the photoswitches and spacers: Mole ratio dependence

While the STM images of the co-assembled networks presented in Figure 4 were obtained using equimolar mixtures of the spacer and the switch, it is possible to vary the ratio of the two components in solution to influence the percentage of surface adsorbed switches. The control over the surface composition could be exercised better when using **u_2DiMeF** as the spacer, plausibly in view of relatively weaker π-stacking interactions compared to other fluorene-based spacers (*vide infra*). Variation of spacer/switch ratio in favor of the switch, led to an increasing surface coverage of the bright features as depicted in STM images provided in Figure 5a–c which further confirm that the bright features observed in STM images are the photoswitches merged within the SAMNs. To quantify the surface coverage of the switches, the bright features were counted for the first STM scan in a new area on the surface. Figure 5d shows the percentage switch count per 100 nm^2 against the mole fraction of **u_2Sw** in solution. The linear trend observed in the plot demonstrates that the number of switches adsorbed on the surface is adjustable in a controlled manner. It is important to note that the switch count on the surface is significantly lower than its fraction in solution, possibly originating from the higher surface affinity of the **u_2DiMeF** spacer. Additional data on the

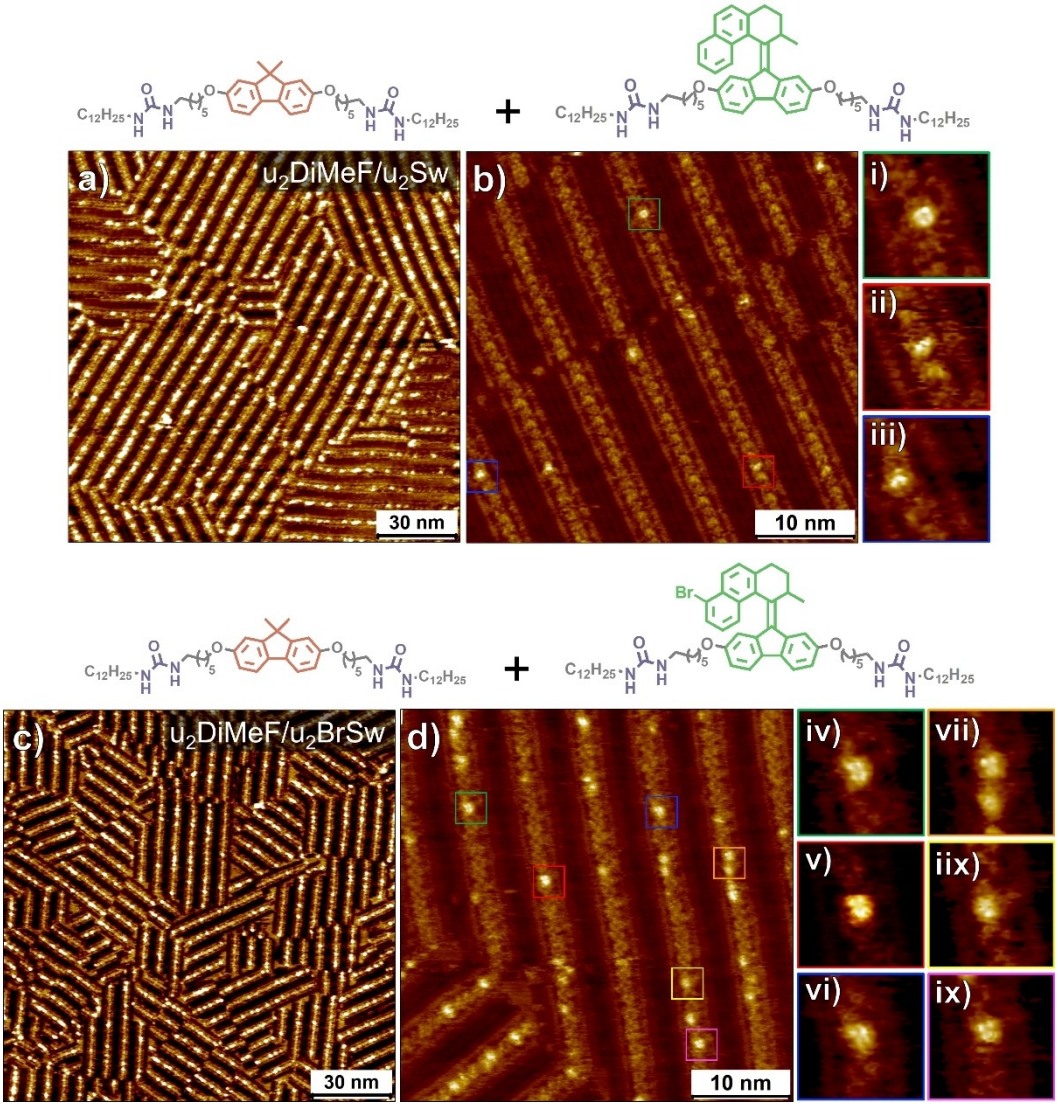

Figure 4. Co-assembly of the u_2DiMeF spacers with the bis-urea (u_2Sw)- and brominated bis-urea switch (u_2BrSw). (a, b) Large, and small scale STM images of the u_2DiMeF/u_2Sw system (1 : 1 ratio with a total concentration of 0.31 mM). The colored squares in (b) highlight a few isolated switch molecules (i-iii). The corresponding magnified areas provided next to the STM image. (c, d) Large, and small scale STM images of the u_2DiMeF/u_2BrSw system (1 : 1 ratio with a total concentration of 0.31 mM). The colored squares in (d) highlight a few isolated switch molecules. The corresponding magnified areas provided next to the STM image (iv–ix). (a–d) $V_{bias} = -0.80$ V, $I_{set} = 0.05$ nA.

switch counts can be found in Table S7 in the supporting information.

To understand if there is any clustering of molecular switches as a function of the spacer-to-switch ratio, we carried out the nearest neighbor (NN) distance analysis by considering the distribution of switches immobilized along the column axis. This analysis was applied to the STM images provided in 5a–c, and resulted in a histogram of relative frequencies as shown in Figure S18 in the supporting information. Comparing the relative frequencies for distances between neighboring immobilized switches for different spacer-to-switch ratios revealed that both 3 : 1 and 1 : 1 ratios share a similar frequency (~10%) for a distance of around 1.5 nm, while it is substantially higher for the 1 : 3 spacer-to switch ratio (~33%) indicating clustering of switches within a given column as expected from the higher amount of switches in the latter case. However, for a distance of around 2.5 nm, all three ratios share an almost equal frequency (~25%) which is the highest for both the 3 : 1 and 1 : 1 ratios. The NN analysis thus indicates that the optimal average distance for the co-assembly of spacer and switch molecules is around 2.5 nm irrespective of the mole ratio used. For an average spacing of around 1.5 nm (and smaller), the assembly can be stable only up to a certain frequency, as a too-high frequency would imply a lack of enough spacer molecules to stabilize photoswitches as is the case for 1 : 3 spacer-to-switch ratio.

Modeling was also performed for co-assembled systems in order to understand the role of the intermolecular interactions in the stabilization of the photoswitches, to investigate the optimal number of spacer molecules between two switch

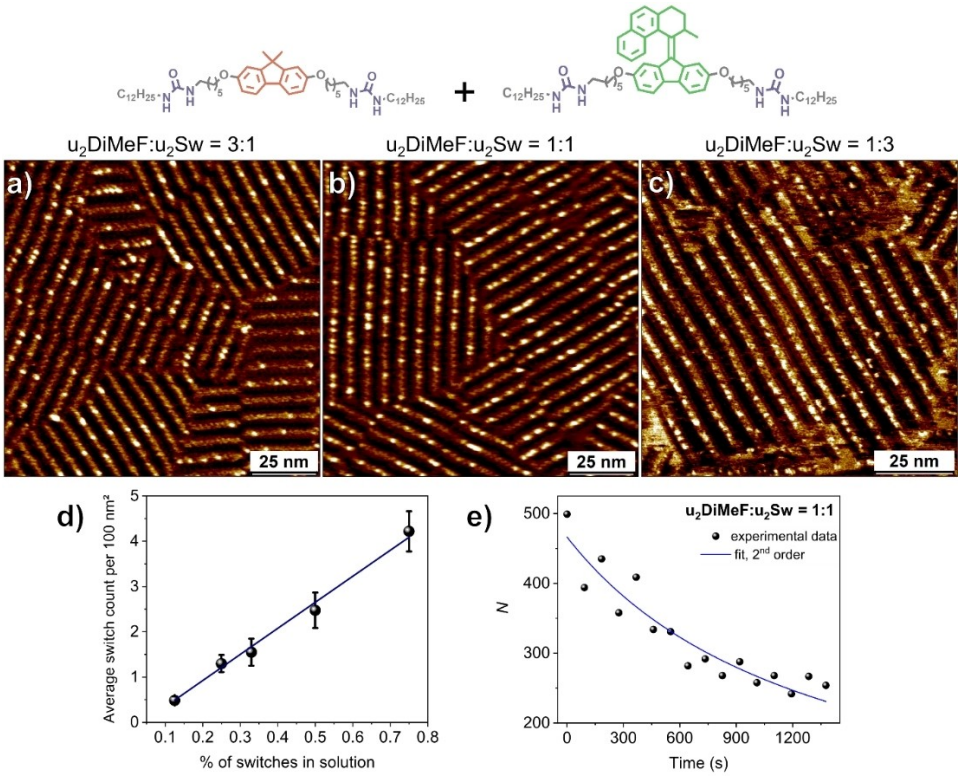

Figure 5. Mole ratio dependence and scanning induced desorption of photoswitches at the solution-solid interface at a total concentration of 0.31 mM for the u_2DiMeF/u_2Sw system. (a-c) Representative STM images at different spacer:switch ratios. An increase in the amount of the photoswitch in solution leads to an increase in the surface coverage of the switch. $V_{bias} = -0.80$ V, $I_{set} = 0.05$ nA. (d) Variation of the average switch count as a function of the percentage of the switch in solution. (e) Scanning induced desorption of the photoswitches. The decrease in the switch count (*N*) is fitted to second-order kinetics using nonlinear least-squares fit[71] for $V_{bias} = -0.80$ V, $I_{set} = 0.05$ nA.

molecules, and to study the interaction between their cores. Three different surface compositions with varying **u_2DiMeF** to **u_2Sw** ratios were studied. Based on the previously discussed calculations for the self-assembled spacer (*vide supra*), only the edge-on conformation of both switch and spacer molecules, with the urea groups pointing in the same direction, was considered. The model of the 1:1 system consists of alternating spacer and switch molecules co-assembled on single-layer graphite, while the 2:1 and 3:1 model systems sandwich two (or three) spacer molecules in between two switch molecules. Optimized structures of co-assembled monolayers (Figure 6 a-c) show that the main driving force for their stabilization is the formation of hydrogen bonding between the urea groups of the switch and spacer molecules. Additionally, the presence of the long alkyl chains helps to stabilize the monolayer and enables better interaction between the graphitic surface and the self-assembly. Together, these results nicely show that utilized supramolecular design principles hold.

Interestingly, the optimized structures for different **u_2DiMeF** to **u_2Sw** ratios exhibit a degree of disorder larger than in the case of switch-free **u_2DiMeF**. This disorder seems to be a consequence of steric hindrance between the methyl groups in the core of the spacer molecule and the rotor of the switch. These local geometrical constraints propagate disorder in the network, which can provide additional mobility for the molecules that could explain the difficulty in obtaining sub-molecular resolution in STM experiments of these systems. The core of the spacer is forced to tilt parallel to the surface (average tilt angle: 44°) in the 1:1 (**u_2DiMeF**:**u_2Sw**) system, to reduce the steric hindrance between the methyl groups of the spacer core and the switch, while maintaining the hydrogen-bonded network (Figure 6a, Table S5 in the supporting information). As the ratio of **u_2DiMeF** towards **u_2Sw** increases to 2:1, the cores can maintain the edge-on conformation to a larger extent (average tilt angle: 79°, Table S5 in the supporting information), due to increased free volume around the switch, further supporting the original design principle for achieving co-assembly capable of uniform motion (Figure 6b). Adding additional spacer molecules to the co-assembly (3:1, **u_2DiMeF**:**u_2Sw**) leads to the formation of noticeable gaps in the network where the hydrogen-bonded co-assembly breaks (Figure 6c). In theory, increasing the number of spacer molecules would "dilute" the steric hindrance between the spacer and switch cores and could therefore additionally stabilize the system. However, as we proceed to the 3:1 ratio, hydrogen bonding between the spacer molecules becomes the dominant molecule-molecule interaction, and the bis-urea moieties form very directional H-bonds. Therefore, there is a lesser possibility for conformational change that could counteract the geometrical constraints originating from the core-core interactions. Consequently, it seems there is an optimal number of spacers that would allow the formation of a well-defined compact hydro-

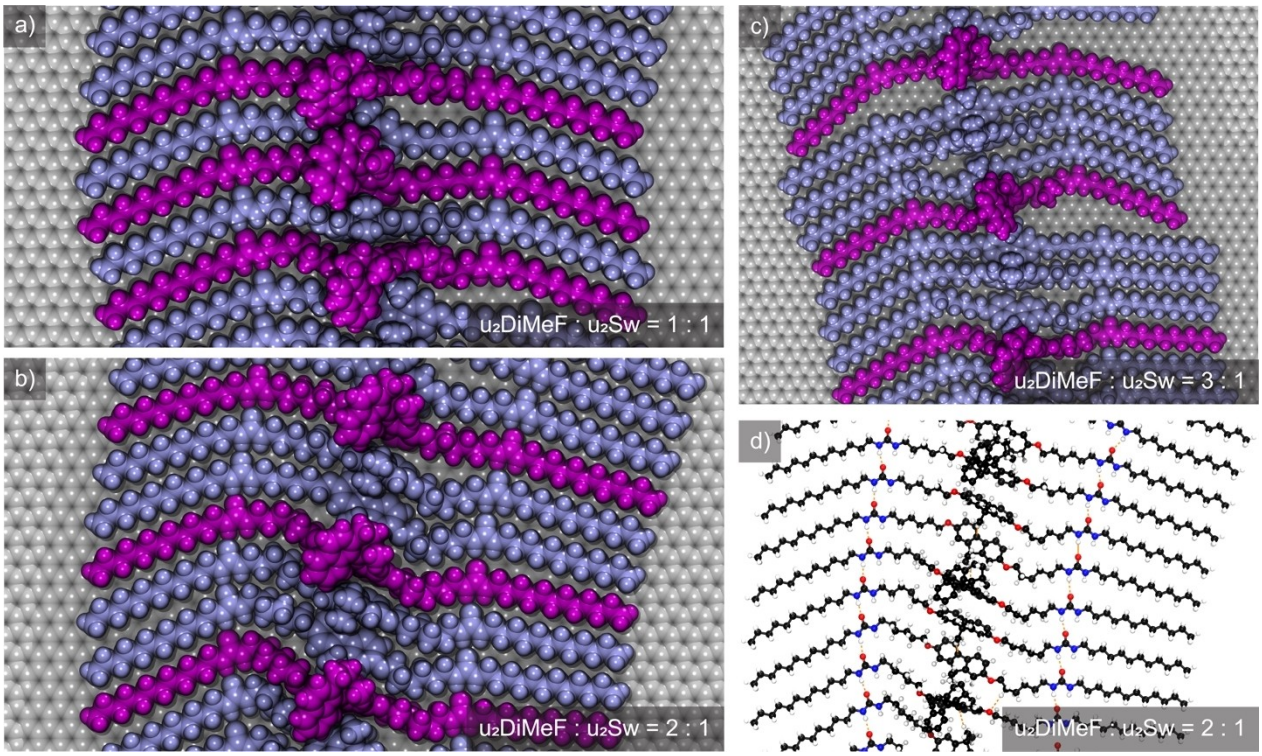

Figure 6. MD optimized molecular models for the SAMNs formed by the co-assembly of bis-urea spacers (u_2DiMeF, light purple) and photoswitches (u_2Sw, magenta) in 1:1 ratio (a), 2:1 ratio (b) and 3:1 ratio (c). It is clear from the models that the 2:1 ratio leads to the most densely packed network, whose hydrogen bonding is indicated in orange in (d).

gen-bonded network, which for the studied co-assembly corresponds to the 2:1 (**u_2DiMeF**:**u_2Sw**) ratio. Geometrical analysis of the spacer core tilt and further analysis of **u_2DiMeF** and **u_2Sw** co-assembly is provided in the supporting information (section 4.3.).

A very important observation for all co-assembled structures optimized is the achievement of the edge-on conformations for the switch molecule. This is a significant finding as the switch molecule must be in a proper orientation to be able to perform unhindered motion. The results of the MD calculations show that the use of a spacer molecule is a very effective way to create the required free volume around the rotor. Furthermore, they show that the spacer core to surface tilt angle can be modulated by varying the molecule ratio, which yields flexibility in the conformation of the co-assembled network, ensuring the proper switch orientation.

Co-assembly of the photoswitches and spacers: STM scanning induced desorption

During the investigation of the **u_2DiMeF/u_2Sw** system, we observed gradual decrease in the switch count when scanning the same area during a few minutes (see Figure S10 in the supporting information). This indicates a desorption of the molecular switches as a function of time. Furthermore, it was found that switches in domains oriented at an acute angle towards the fast scanning axis desorb faster than switches in domains at an obtuse angle (Figure S11 in the supporting information). For the surface-anchored photoswitch design, such fast desorption of the photoswitches is not desired. Since the self-assembly at the solution-solid interface is characterized by both in-plane and out-of-plane dynamics, the desorption of the switches at RT is plausible. However, since the data is obtained while continuously scanning with the STM tip, it is important to differentiate the inherent adsorption-desorption dynamics from the STM scanning-induced desorption dynamics. The STM tip is known to exert significant lateral forces on the self-assembled monolayers and thus may remove molecules, particularly those that are adsorbed orthogonal to the substrate surface. The switch count was found to decrease upon continuously scanning the same area. A rapid decrease in the switch count was observed for the first 10 minutes followed by a more gradual decrease for the 1:1 **u_2DiMeF/u_2Sw** system (Figure 5e).

Co-assembly of the photoswitches and spacers: other systems

The co-assembly of other bis-urea spacer designs involving fluorene (**u_2F**) and fluorenone (**u_2OF**) cores was also investigated together with the photoswitches (see Figure S12 in the supporting information). None of these combinations were found to be as promising as the ones involving **u_2DiMeF**. For example, deposition of solution mixtures containing **u_2OF** spacer and **u_2Sw** yielded SAMNs with preferential adsorption of

the spacer. Low concentrations of **u_2OF** led to dynamic monolayers unstable to STM imaging whereas at intermediate concentrations of the spacer, no-co-adsorption of the switch within the monolayers of the spacer was observed (Figures S13 in the supporting information). Similar observations were made for the co-assembly of **u_2F** spacer and **u_2Sw**. Co-assembly of the spacer based on only ureidoalkyl chains **u_2A** with the brominated ureidoalkyl switch **u_2BrSw** provided mixed monolayers with random insertion of the photoswitches in the lamellae, however, obtaining molecular resolution STM images of these SAMNs was relatively more challenging.

The co-assembly of the bis-alkyl dimethylfluorene spacer (**a_2DiMeF**) with the bis-alkyl brominated switch (**a_2BrSw**) provided a completely different scenario. The SAMNs consisted of two types of domains: one made up of only **a_2BrSw** whereas the other domains contained **a_2BrSw** dispersed within the domains of **a_2DiMeF** (Figures S14 in the supporting information). The phase-separated **a_2BrSw** domains accounted for about 30% of the surface coverage. The insertion of **a_2BrSw** within the **a_2DiMeF** lamellae appears to be non-random. The switch count was found to be considerably higher (Table S7 in supporting information) than for any other system despite the partial occupation of the surface by switch domains mainly due to the smaller unit cell of the structure. Detailed analysis of this system in terms of STM scanning induced desorption was not carried out.

Mixing the monourea switch **auBrSw** with the monourea spacer **auDiMeF** resulted in the formation of lamellar structures. The lamellae showed the end-to-end packing of the urea containing side chains whereas interdigitation on the alkyl side chains (Figures S15 in the supporting information). The switch count was found to be lower than that in bis-urea systems (Table S7 in the supporting information). The mobility of the switches in the co-assembled networks was found to be high with switches desorbing and readsorbing quickly. This is reflected in a slower overall desorption rate of the switches, so that the switch count only drops to approximately 80% after continued scanning (Figure S16 in the supporting information).

Co-assembly of the photoswitches and spacers: Directionality

For future photoisomerization studies of the molecular switches, it is important to characterize the directionality of the rotors when merged within the spacer lamellae. The rotor makes the switches asymmetrical (*i.e.* helical structure) because it is pointing towards one of the two side chains when adsorbed on the surface. This structural feature is anticipated to be reflected in the STM images of the switches. Thus, the high-resolution STM images of the switch-spacer combinations were analyzed carefully to assign directionality in the orientation of the switches immobilized within spacer lamellae. The distance of the switch from the bis-urea ridge was measured from calibrated STM images. Additional information on the analysis can be found in Figure S17 in the supporting information. These distances were measured for several bright features across different STM images. The numbers indicate that most molecular switches are positioned in an off-centered manner within spacer lamella as also visually evident from the STM image provided in Figure 7a. This was found to be the case for the bis-

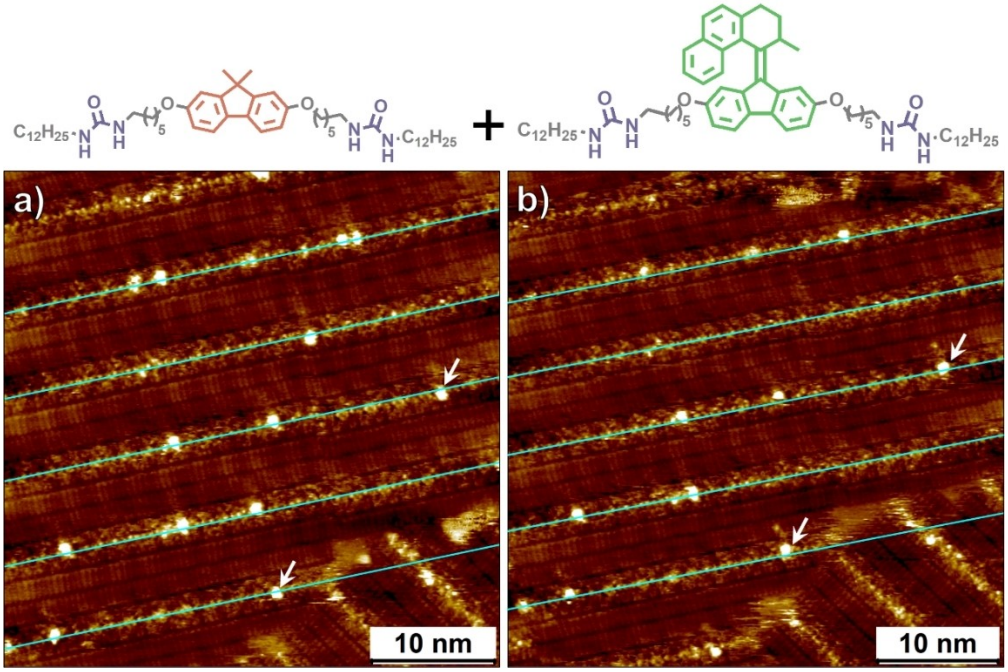

Figure 7. Subsequently obtained STM images showing the directionality of the photoswitches, and tip induced changes in the positioning of the switches within the spacer lamellae in the u_2DiMeF/u_2Sw system. (a) The cyan lines drawn through the STM image define the axis of the lamella which was used as a reference to define the position of the switches within the column. It is evident that most photoswitches are positioned in an off-centered manner. (b) STM image obtained immediately after the one provided in (a). A few switches have desorbed while the ones indicated by white arrows have changed their position from one side to the other side of the lamella. Imaging parameters (a, b): $V_{bias} = -0.80$ V, $I_{set} = 0.05$ nA.

urea as well as the brominated bis-urea switches. Furthermore, we are also carrying out a detailed analysis to understand STM-tip-induced movement within the surface-adsorbed switches to be able to differentiate it from the photoisomerization of the molecular switches in future studies. Preliminary analysis of sequentially obtained STM images indicates that while the STM tip does move the switches from an off-center position on one side of the column to the other side, the percentage occurrence of such movement is negligible (Figure 6a–b). The two enantiomers, namely the *P* and the *M* helices, could not be distinguished in the high-resolution STM images. The bromination of the switch, which was carried out to enhance the observation of such directionality by acting as an extension of the rotor that reaches over the center of the column, did not fundamentally change the STM resolution, but provided reproducible and better STM contrast compared to its non-brominated counterpart.

Conclusions and Outlook

We have presented above a strategy to immobilize overcrowded alkene photoswitches within physisorbed self-assembled monolayers. The decoupling of the rotor from the surface was achieved using hydrogen-bonded bis-urea units whereas the challenge of steric crowding was resolved using precisely designed spacer molecules. The STM data revealed that the switches are merged within the matrix of the spacer lamellae. The orthogonal orientation of the switches with respect to the surface was confirmed by comparing the MM-predicted structures and the STM results. Detailed investigation of multiple spacer and switch designs allowed us to settle in on the most appropriate spacer/switch combination which not only enabled seamless merging of photoswitches within spacer monolayers but also permitted sub-molecular resolution imaging of the rotors which is essential for studying photoswitching behavior in the future.

One of the key challenges in the realization of devices based on surface-confined molecular motors and switches is the development of effective strategies for their immobilization on solid surfaces. The spacer-switch design presented in this work, which is inspired from natural systems where rotary motors and switches are often embedded within cellular membranes, bodes well for interfacing the nanoscale rotary motion to the macroscopic world. The use of robust and highly directional hydrogen bonding interactions between bis-urea units used for the immobilization is also a highly potent strategy to overcome the incoherence usually observed in the solution phase. The high-resolution STM imaging supported by detailed MM and MD simulations is a promising approach for the in-depth characterization of the physisorbed molecular motors and switches.

Having successfully established the surface immobilization strategy in this work, our future studies will focus on investigating the irradiation induced photoswitching in some of these systems. In contrast to UHV conditions, where the motion of isolated single molecules can be readily tracked, the solution-solid interface offers a much complex environment due to its dynamic nature. As mentioned earlier, one has to be extremely careful to separate the tip induced dynamics from the photoinduced switching. To this end, systematic analysis of the sequentially obtained STM images is in progress to thoroughly characterize the former. This will be followed by *in-situ* photoirradiation experiments carried out at the solution-solid interface. Despite the experimental challenges involved in the high-resolution characterization of single molecule switching behavior at the solution-solid interface, we strongly believe that the design established here provides a solid basis and will be a key strategy in harnessing the directional rotary motion of surface bound motors and switches.

Supporting Information

The Supporting Information is available free of charge at https://pubs.acs.org/doi/.

Experimental materials and methods, NMR data, details of the molecular mechanics and molecular dynamics simulations, additional and supporting STM data as well as supporting data from the simulations. (PDF)

Notes

The authors declare no competing financial interest.

Acknowledgements

Marco Ovalle is acknowledged for making the TOC graphic. This work is supported by the European Union (H2020 Excellent Science – European Research Council) under grant number 694345 (B.L.F. and C.S.); Ministerie van Onderwijs, Cultuur en Wetenschap (Ministry of Education, Culture and Science, Netherlands) under Gravitation Program grant number 024.001.035 (B.L.F.). The authors also gratefully acknowledge financial support from the Research Foundation – Flanders (FWO G0E3422 N), KU Leuven – Internal Funds (C14/23/090). This work was in part supported by FWO under EOS 40007495. T. R. acknowledges financial support through a FWO PhD fellowship fundamental research (fellowship 11F2422N).

Conflict of Interests

The authors declare no conflict of interest.

Data Availability Statement

The data that support the findings of this study are available from the corresponding author upon reasonable request.

Keywords: *bis*-urea · molecular motors · overcrowded alkenes · scanning tunneling microscopy · self-assembly

[1] T. Aida, E. W. Meijer, S. I. Stupp, *Science* **2012**, *335*, 813–817.
[2] J.-M. Lehn, *Angew. Chem. Int. Ed.* **2013**, *52*, 2836–2850.
[3] D. S. Goodsell, *The Machinery of Life*, Copernicus New York, NY, **2009**, p 9-25.
[4] E. Busseron, Y. Ruff, E. Moulin, N. Giuseppone, *Nanoscale* **2013**, *5*, 7098–7140.
[5] Y. Zhao, S. Ippolito, P. Samorì, *Adv. Opt. Mater.* **2019**, *7*, 1900286.
[6] E. Mattia, S. Otto, *Nat. Nanotechnol.* **2015**, *10*, 111–119.
[7] D. B. Amabilino, D. K. Smith, J. W. Steed, *Chem. Soc. Rev.* **2017**, *46*, 2404–2420.
[8] C. K. McLaughlin, G. D. Hamblin, H. F. Sleiman, *Chem. Soc. Rev.* **2011**, *40*, 5647–5656.
[9] K. Kinbara, T. Aida, *Chem. Rev.* **2005**, *105*, 1377–1400.
[10] K. Ariga, Y. Yonamine, J. P. Hill in *Functional Nanomaterials Prepared by Nanoarchitectonics-Based Supramolecular Assembly* (Eds.: M. Bardosova, T. Wagner), Springer Netherlands, Dordrecht, **2015**, pp. 45–61.
[11] J. A. A. W. Elemans, S. Lei, S. De Feyter, *Angew. Chem. Int. Ed.* **2009**, *48*, 7298–7332.
[12] J. F. Stoddart, *Angew. Chem. Int. Ed.* **2017**, *56*, 11094–11125.
[13] J.-P. Sauvage, *Angew. Chem. Int. Ed.* **2017**, *56*, 11080–11093.
[14] B. L. Feringa, *Angew. Chem. Int. Ed.* **2017**, *56*, 11060–11078.
[15] Z.-T. Shi, Q. Zhang, H. Tian, D.-H. Qu, *Adv. Intell. Syst.* **2020**, *2*, 1900169.
[16] F. Lancia, A. Ryabchun, N. Katsonis, *Nat. Chem. Rev.* **2019**, *3*, 536–551.
[17] W. R. Browne, B. L. Feringa, *Chiroptical Molecular Switches*, Wiley-VCH Verlag GmbH & Co. KGaA, Weinheim **2011**, pp. 121–179.
[18] A. Coskun, M. Banaszak, R. D. Astumian, J. F. Stoddart, B. A. Grzybowski, *Chem. Soc. Rev.* **2012**, *41*, 19–30.
[19] V. García-López, D. Liu, J. M. Tour, *Chem. Rev.* **2020**, *120*, 79–124.
[20] J. D. Harris, M. J. Moran, I. Aprahamian, *Proc. Natl. Acad. Sci. USA* **2018**, *115*, 9414–9422.
[21] S. Erbas-Cakmak, D. A. Leigh, C. T. McTernan, A. L. Nussbaumer, *Chem. Rev.* **2015**, *115*, 10081–10206.
[22] S. Mena-Hernando, E. M. Pérez, *Chem. Soc. Rev.* **2019**, *48*, 5016–5032.
[23] R. S. Forgan, J.-P. Sauvage, J. F. Stoddart, *Chem. Rev.* **2011**, *111*, 5434–5464.
[24] D. R. S. Pooler, A. S. Lubbe, S. Crespi, B. L. Feringa, *Chem. Sci.* **2021**, *12*, 14964–14986.
[25] D. Dattler, G. Fuks, J. Heiser, E. Moulin, A. Perrot, X. Yao, N. Giuseppone, *Chem. Rev.* **2020**, *120*, 310–433.
[26] M. Jeong, J. Park, S. Kwon, *Eur. J. Org. Chem.* **2020**, *2020*, 7254–7283.
[27] S. Yokoyama, T. Hirose, K. Matsuda, *Chem. Eur. J.* **2015**, *21*, 13569–13576.
[28] R. A. Bissell, E. Córdova, A. E. Kaifer, J. F. Stoddart, *Nature* **1994**, *369*, 133–137.
[29] A. Goujon, T. Lang, G. Mariani, E. Moulin, G. Fuks, J. Raya, E. Buhler, N. Giuseppone, *J. Am. Chem. Soc.* **2017**, *139*, 14825–14828.
[30] T. Kudernac, N. Ruangsupapichat, M. Parschau, B. Macia, N. Katsonis, S. R. Harutyunyan, K.-H. Ernst, B. L. Feringa, *Nature* **2011**, *479*, 208–211.
[31] P. Štacko, J. C. M. Kistemaker, T. v. Leeuwen, M.-C. Chang, E. Otten, B. L. Feringa, *Science* **2017**, *356*, 964–968.
[32] J. Berná, D. A. Leigh, M. Lubomska, S. M. Mendoza, E. M. Pérez, P. Rudolf, G. Teobaldi, F. Zerbetto, *Nat. Mater.* **2005**, *4*, 704–710.
[33] S. Saha, J. F. Stoddart, *Chem. Soc. Rev.* **2007**, *36*, 77–92.
[34] R. D. Astumian, *Phys. Chem. Chem. Phys.* **2007**, *9*, 5067–5083.
[35] J. C. Love, L. A. Estroff, J. K. Kriebel, R. G. Nuzzo, G. M. Whitesides, *Chem. Rev.* **2005**, *105*, 1103–1170.
[36] Q. Zhang, D.-H. Qu, *ChemPhysChem* **2016**, *17*, 1759–1768.
[37] V. Balzani, A. Credi, M. Venturi, *ChemPhysChem* **2008**, *9*, 202–220.
[38] M. M. Pollard, M. Lubomska, P. Rudolf, B. L. Feringa, *Angew. Chem. Int. Ed.* **2007**, *46*, 1278–1280.
[39] J. Chen, K.-Y. Chen, G. T. Carroll, B. L. Feringa, *Chem. Commun.* **2014**, *50*, 12641–12644.
[40] G. T. Carroll, M. M. Pollard, R. van Delden, B. L. Feringa, *Chem. Sci.* **2010**, *1*, 97–101.
[41] K.-Y. Chen, O. Ivashenko, G. T. Carroll, J. Robertus, J. C. M. Kistemaker, G. London, W. R. Browne, P. Rudolf, B. L. Feringa, *J. Am. Chem. Soc.* **2014**, *136*, 3219–3224.
[42] R. A. van Delden, M. K. J. ter Wiel, M. M. Pollard, J. Vicario, N. Koumura, B. L. Feringa, *Nature* **2005**, *437*, 1337–1340.
[43] N. Koumura, R. W. J. Zijlstra, R. A. van Delden, N. Harada, B. L. Feringa, *Nature* **1999**, *401*, 152–155.
[44] B. Krajnik, J. Chen, M. A. Watson, S. L. Cockroft, B. L. Feringa, J. Hofkens, *J. Am. Chem. Soc.* **2017**, *139*, 7156–7159.
[45] K. S. Mali, N. Pearce, S. De Feyter, N. R. Champness, *Chem. Soc. Rev.* **2017**, *46*, 2520–2542.
[46] D. P. Goronzy, M. Ebrahimi, F. Rosei, Arramel, Y. Fang, S. De Feyter, S. L. Tait, C. Wang, P. H. Beton, A. T. S. Wee, P. S. Weiss, D. F. Perepichka, *ACS Nano* **2018**, *12*, 7445–7481.
[47] J. van Esch, S. De Feyter, R. M. Kellogg, F. De Schryver, B. L. Feringa, *Chem. Eur. J.* **1997**, *3*, 1238–1243.
[48] F. S. Schoonbeek, J. H. van Esch, B. Wegewijs, D. B. A. Rep, M. P. de Haas, T. M. Klapwijk, R. M. Kellogg, B. L. Feringa, *Angew. Chem. Int. Ed.* **1999**, *38*, 1393–1397.
[49] K. Tahara, S. Lei, J. Adisoejoso, S. De Feyter, Y. Tobe, *Chem. Commun.* **2010**, *46*, 8507–8525.
[50] C. Arrigoni, G. Schull, D. Bléger, L. Douillard, C. Fiorini-Debuisschert, F. Mathevet, D. Kreher, A.-J. Attias, F. Charra, *J. Phys. Chem. Lett.* **2010**, *1*, 190–194.
[51] D. Bléger, A. Bocheux, D. Kreher, F. Mathevet, A.-J. Attias, G. Metgé, L. Douillard, C. Fiorini-Debuisschert, F. Charra, *Nanoscale* **2013**, *5*, 1452–1455.
[52] M. Yokoya, S. Kimura, M. Yamanaka, *Chem. Eur. J.* **2021**, *27*, 5601–5614.
[53] M. de Loos, B. L. Feringa, J. H. van Esch, *Eur. J. Org. Chem.* **2005**, *2005*, 3615–3631.
[54] A. Gesquière, M. M. S. Abdel-Mottaleb, S. De Feyter, F. C. De Schryver, F. Schoonbeek, J. van Esch, R. M. Kellogg, B. L. Feringa, A. Calderone, R. Lazzaroni, J. L. Brédas, *Langmuir* **2000**, *16*, 10385–10391.
[55] X. Zhang, E. H. Huisman, M. Gurram, W. R. Browne, B. J. van Wees, B. L. Feringa, *Small* **2014**, *10*, 1735–1740.
[56] S. De Feyter, P. C. M. Grim, J. van Esch, R. M. Kellogg, B. L. Feringa, F. C. De Schryver, *J. Phys. Chem. B* **1998**, *102*, 8981–8987.
[57] T. Müller, T. L. Werblowsky, G. M. Florio, B. J. Berne, G. W. Flynn, *Proc. Natl. Acad. Sci. USA* **2005**, *102*, 5315–5322.
[58] R. Reynaerts, A. Minoia, S. M. Gali, L. Daukiya, N. Van Velthoven, D. De Vos, R. Lazzaroni, K. S. Mali, S. De Feyter, *J. Phys. Chem. C* **2020**, *124*, 24874–24882.
[59] N. Koumura, E. M. Geertsema, M. B. van Gelder, A. Meetsma, B. L. Feringa, *J. Am. Chem. Soc.* **2002**, *124*, 5037–5051.
[60] J. C. M. Kistemaker, S. F. Pizzolato, T. van Leeuwen, T. C. Pijper, B. L. Feringa, *Chem. Eur. J.* **2016**, *22*, 13478–13487.
[61] X.-Y. Chen, S. Ozturk, E. J. Sorensen, *Org. Lett.* **2017**, *19*, 1140–1143.
[62] M. V. Ivanov, S. H. Wadumethrige, D. Wang, R. Rathore, *Chem. Eur. J.* **2017**, *23*, 8834–8838.
[63] G. A. Prochazka, *J. Am. Chem. Soc.* **1879**, *1*, 233–260.
[64] J. Wu, W. Liu, L. Liang, Y. Gan, S. Xia, X. Gou, X. Sun, *Tetrahedron Lett.* **2020**, *61*, 151917.
[65] J. Polster, P. Schieberle, *J. Agric. Food Chem.* **2015**, *63*, 1419–1432.
[66] X. Sun, F. Lafolet, G. Lemercier, F. Maurel, J.-C. Lacroix, *J. Phys. Chem. C* **2017**, *121*, 20925–20930.
[67] A. Mukherjee, J. Teyssandier, G. Hennrich, S. De Feyter, K. S. Mali, *Chem. Sci.* **2017**, *8*, 3759–3769.
[68] K. S. Mali, K. Lava, K. Binnemans, S. De Feyter, *Chem. Eur. J.* **2010**, *16*, 14447–14458.
[69] J. M. MacLeod, J. Lipton-Duffin, C. Fu, T. Taerum, D. F. Perepichka, F. Rosei, *ACS Nano* **2017**, *11*, 8901–8909.
[70] J. Teyssandier, S. D. Feyter, K. S. Mali, *Chem. Commun.* **2016**, *52*, 11465–11487.
[71] C. L. Perrin, *J. Chem. Educ.* **2017**, *94*, 669–672.

Manuscript received: November 30, 2023
Version of record online: February 7, 2024